Supporting information

High-density single-atomic Ni-N_4 sites for efficient Fenton-like reactions

Shu-Qi Wang [a,b], Katherine Velez [a], Jiahui Cai [a], Linbo Huang [b], Qing-Hua Zhang [d], Feng Feng [a], Qi An [a, *], Lu Zhao [a, *], Jin-Song Hu [b, c]

a Beijing Key Laboratory of Materials Utilization of Nonmetallic Minerals and Solid Wastes, National Laboratory of Mineral Materials, School of Materials Science and Technology, China University of Geosciences, Beijing 100083, China

b Beijing National Laboratory for Molecular Sciences (BNLMS), CAS Key Laboratory of Molecular Nanostructure and Nanotechnology, Institute of Chemistry, Chinese Academy of Sciences (CAS), Beijing 100190, China

c University of Chinese Academy of Sciences, Beijing 100049, China

d Beijing National Research Center for Condensed Matter Physics, Collaborative Innovation Center of Quantum Matter, Institute of Physics, Chinese Academy of Sciences, Beijing 100190, China.

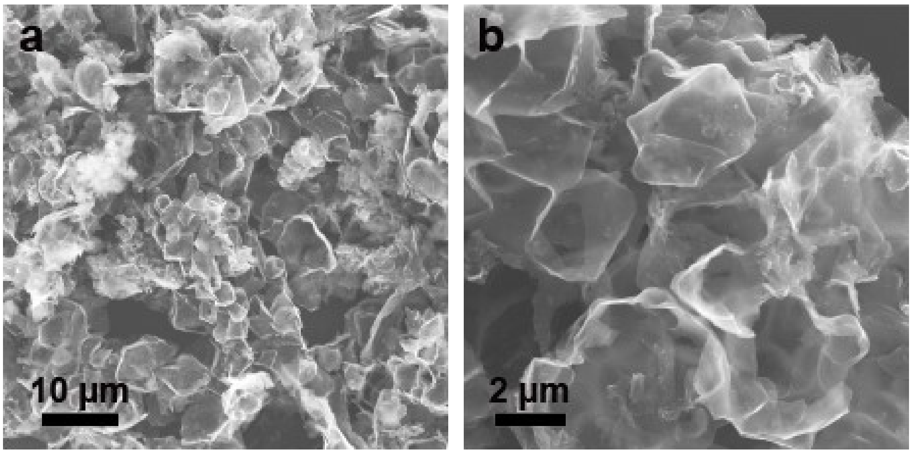

Fig. S1 SEM images of nanoporous carbon with different scale bars.

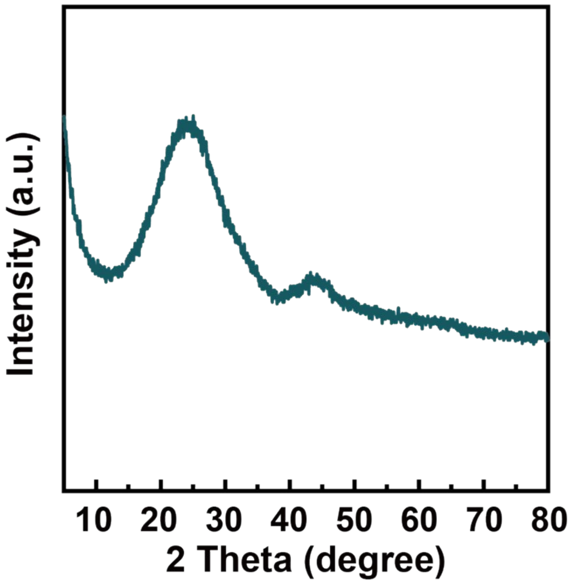

Fig. S2 XRD pattern of nanoporous carbon support.

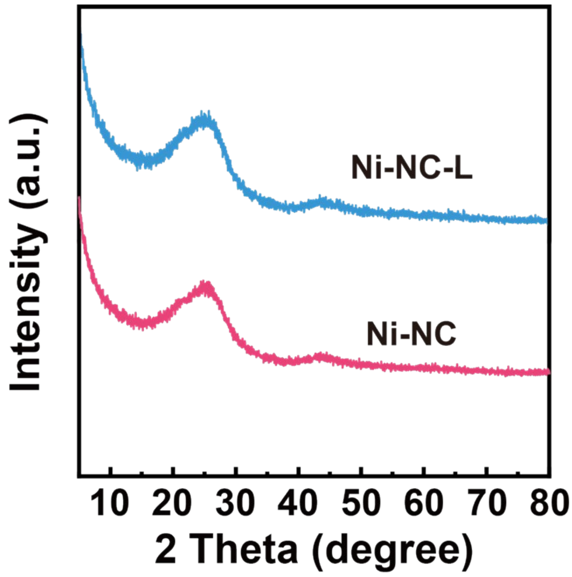

Fig. S3 XRD patterns of Ni-NC-L and Ni-NC catalysts.

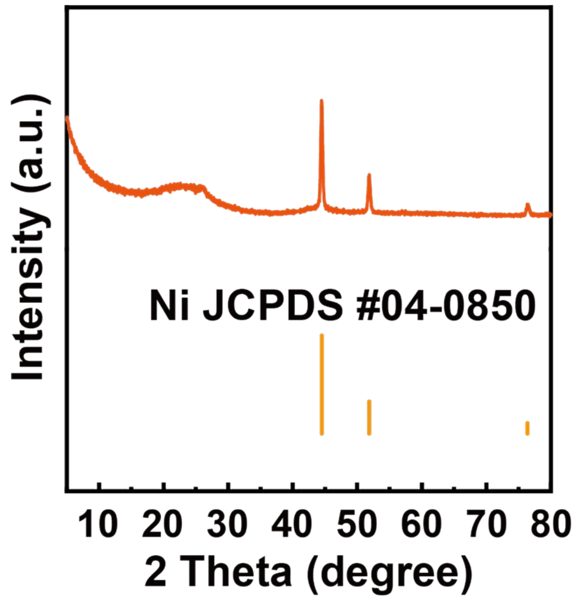

Fig. S4 XRD pattern of Ni NPs/C.

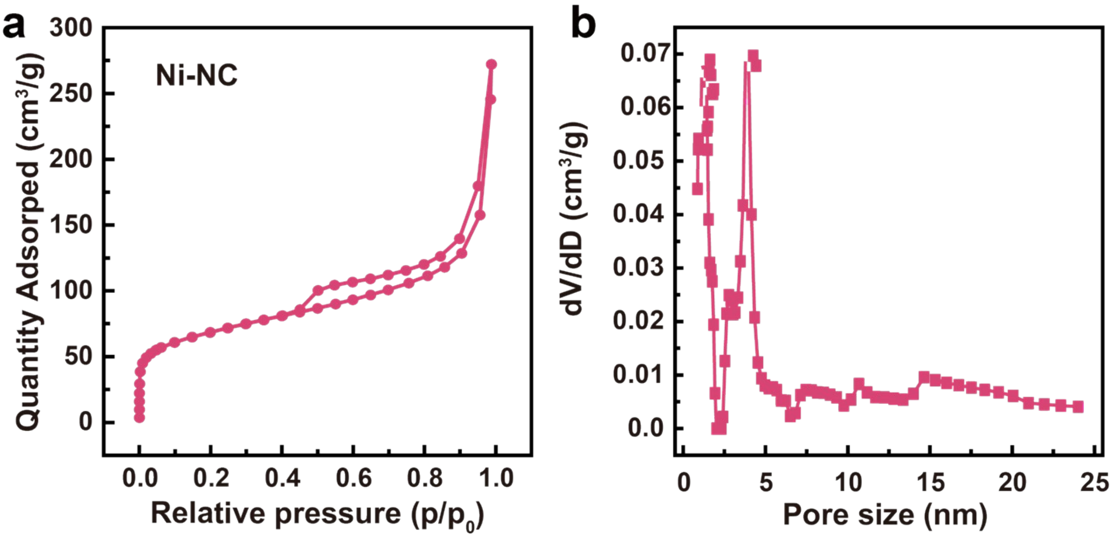

Fig. S5 a, N_2 adsorption-desorption isotherm, and b, corresponding pore size distribution curve of Ni-NC.

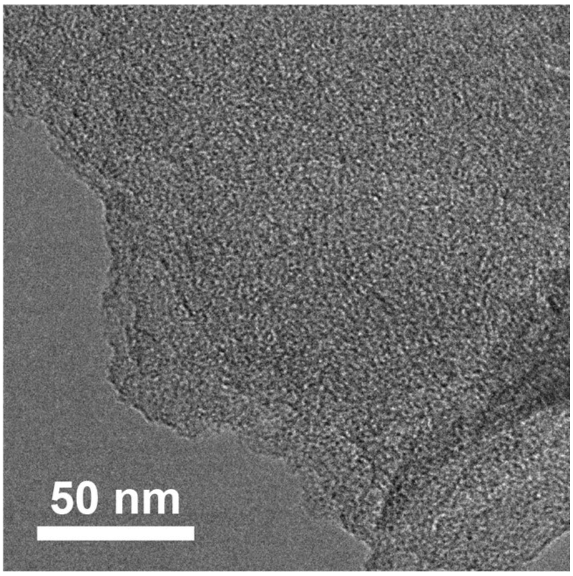

Fig. S6 TEM image of Ni-NC-L.

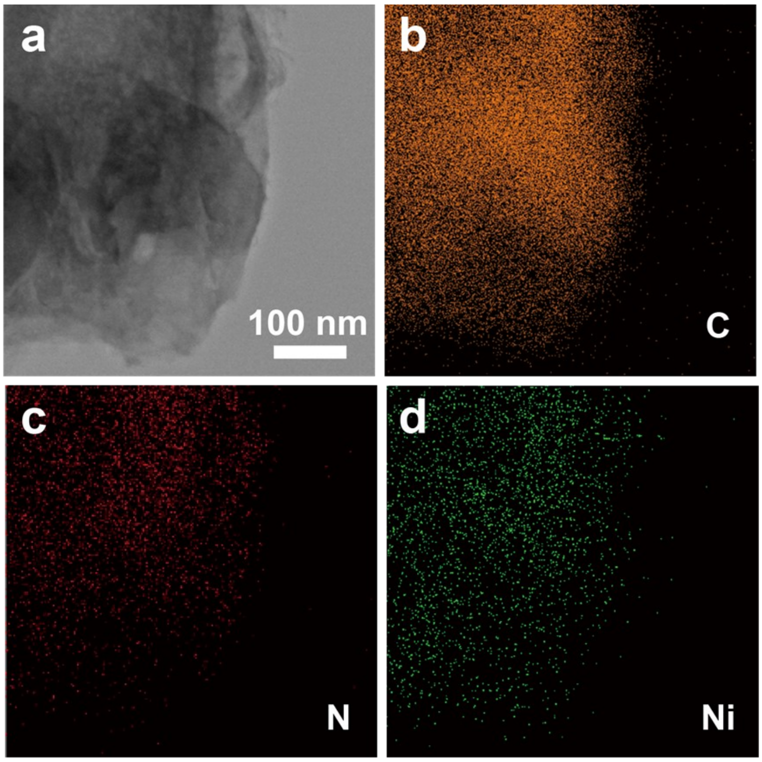

Fig. S7 EDS mapping images of Ni-NC-L.

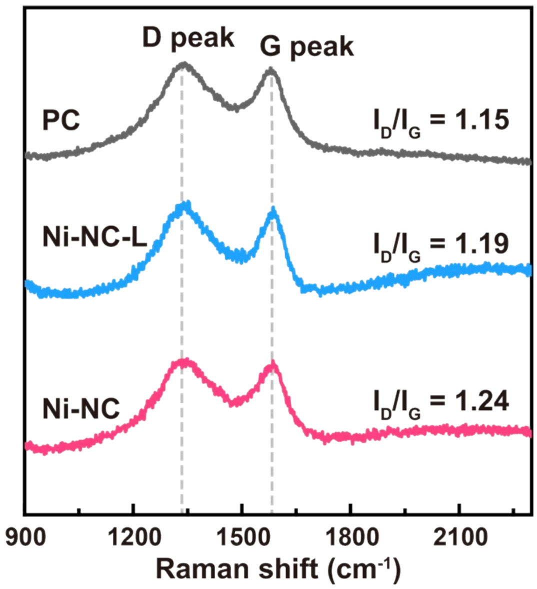

Fig. S8 Raman spectra of Ni-NC, Ni-NC-L and PC.

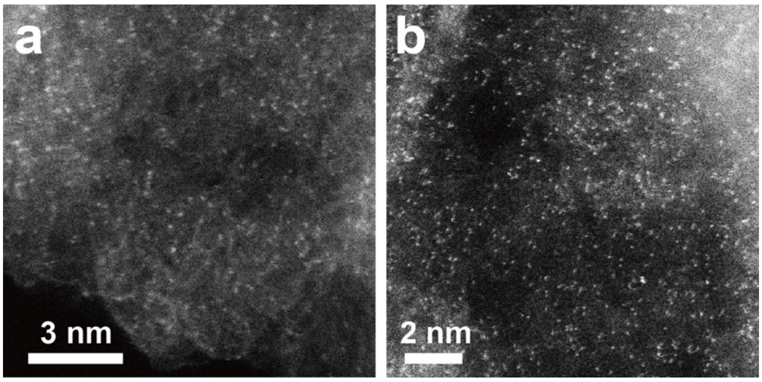

Fig. S9 HAADF-STEM images of Ni-NC.

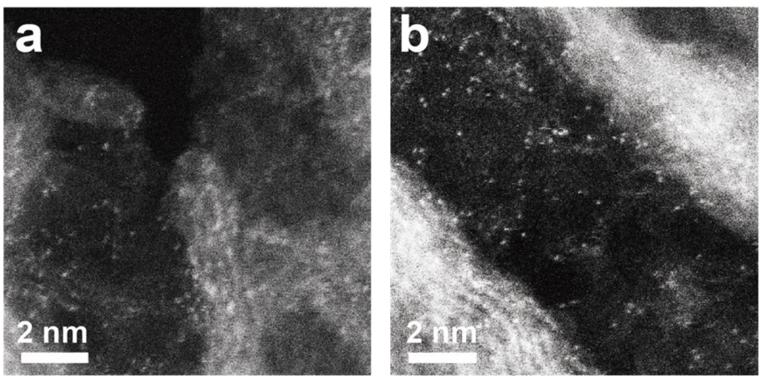

Fig. S10 HAADF-STEM images of Ni-NC-L.

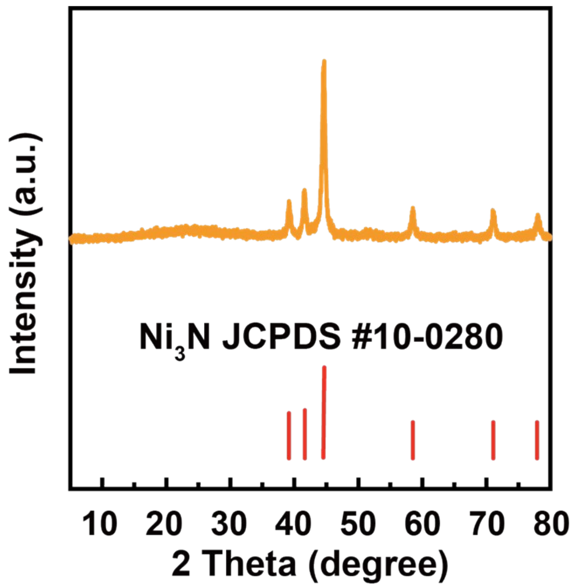

Fig. S11 XRD pattern of Ni_3N/C.

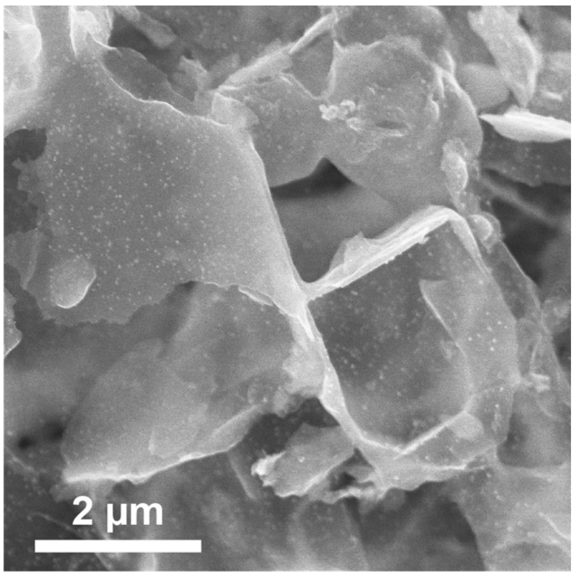

Fig. S12 SEM image of Ni_3N/C.

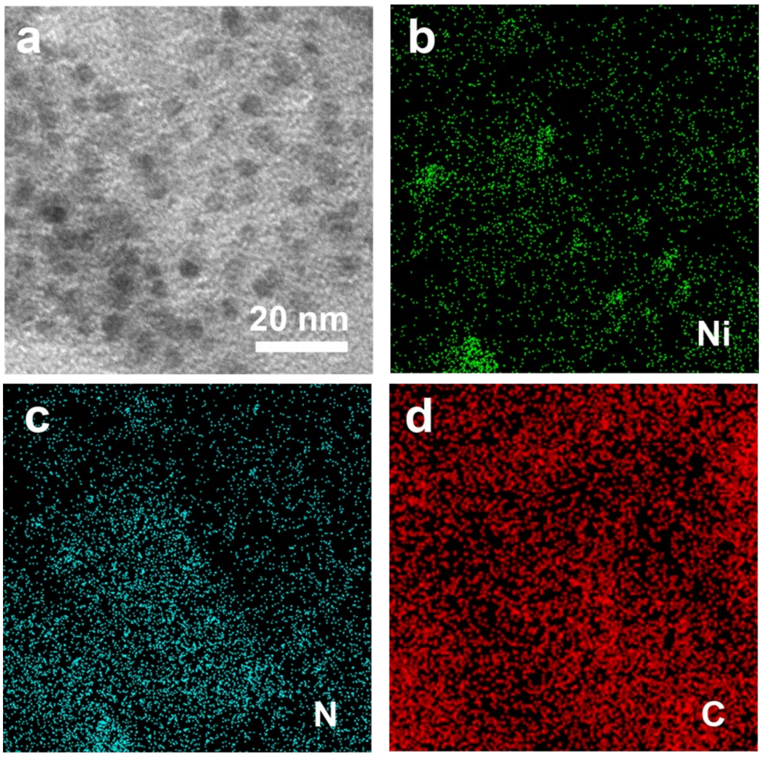

Fig. S13 EDS mapping images of Ni_3N/C.

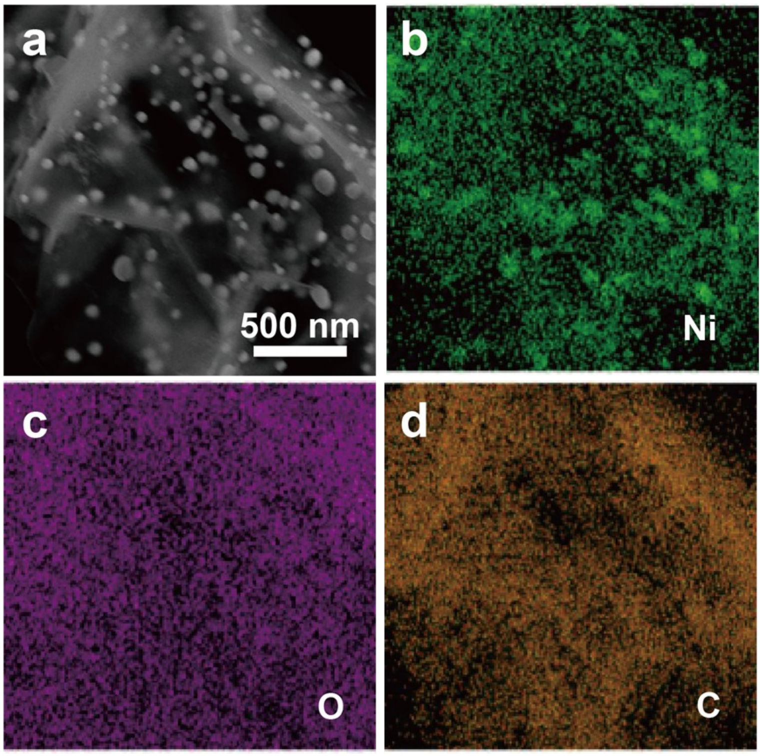

Fig. 14 SEM, and EDS mapping images of NiO/C.

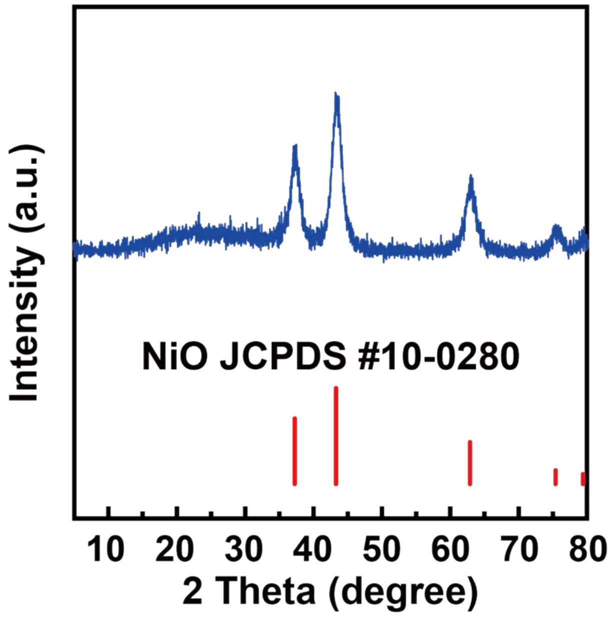

Fig. S15 XRD pattern of NiO/C.

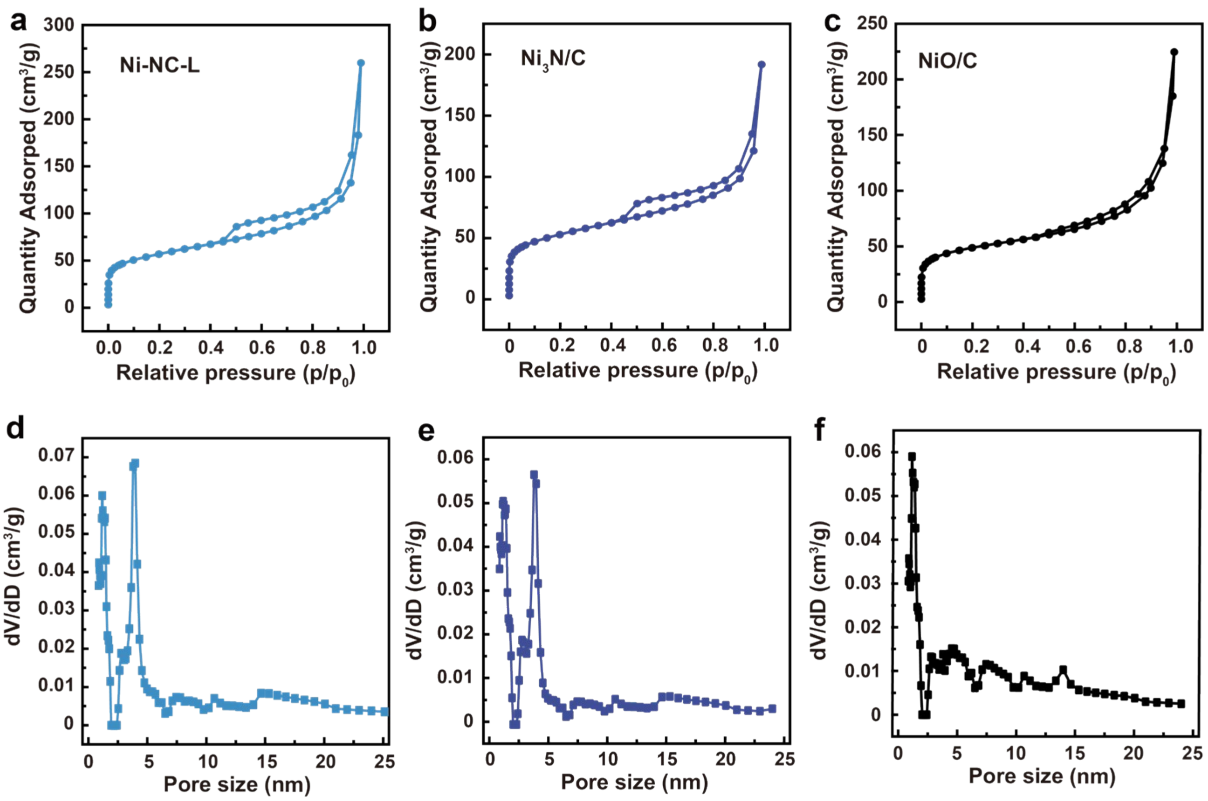

Fig. S16 N_2 adsorption-desorption isotherms of Ni-NC-L (a), Ni_3N/C (b) and NiO/C (c), and corresponding pore size distribution curves of Ni-NC-L (d), Ni_3N/C (e) and NiO/C (f).

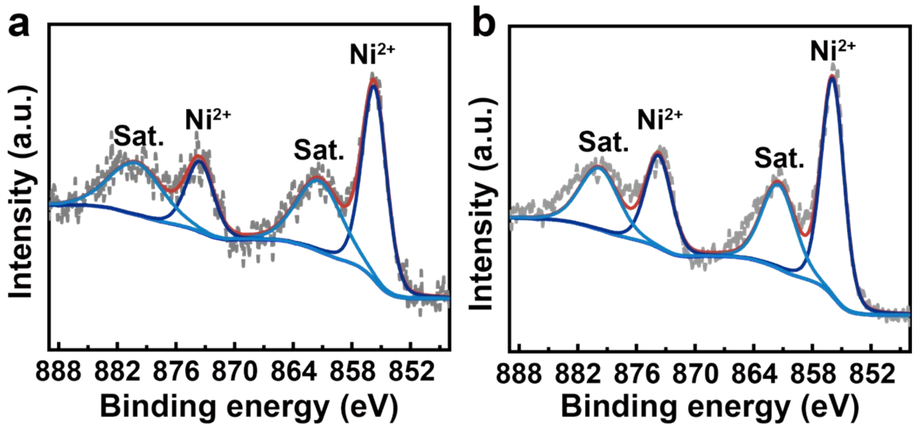

Fig. S17 XPS Ni 2*p* spectra of (a) Ni-NC-L and (b) Ni-NC catalysts.

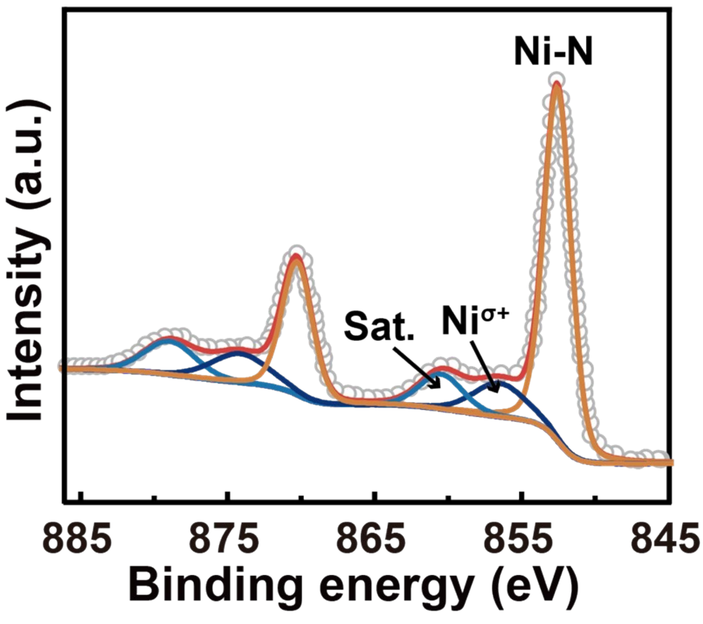

Fig. S18 Ni 2*p* XPS spectrum of Ni_3N/C. The appearance of $Ni^{\sigma+}$ is the result of the oxidation of the catalyst when exposed to air.

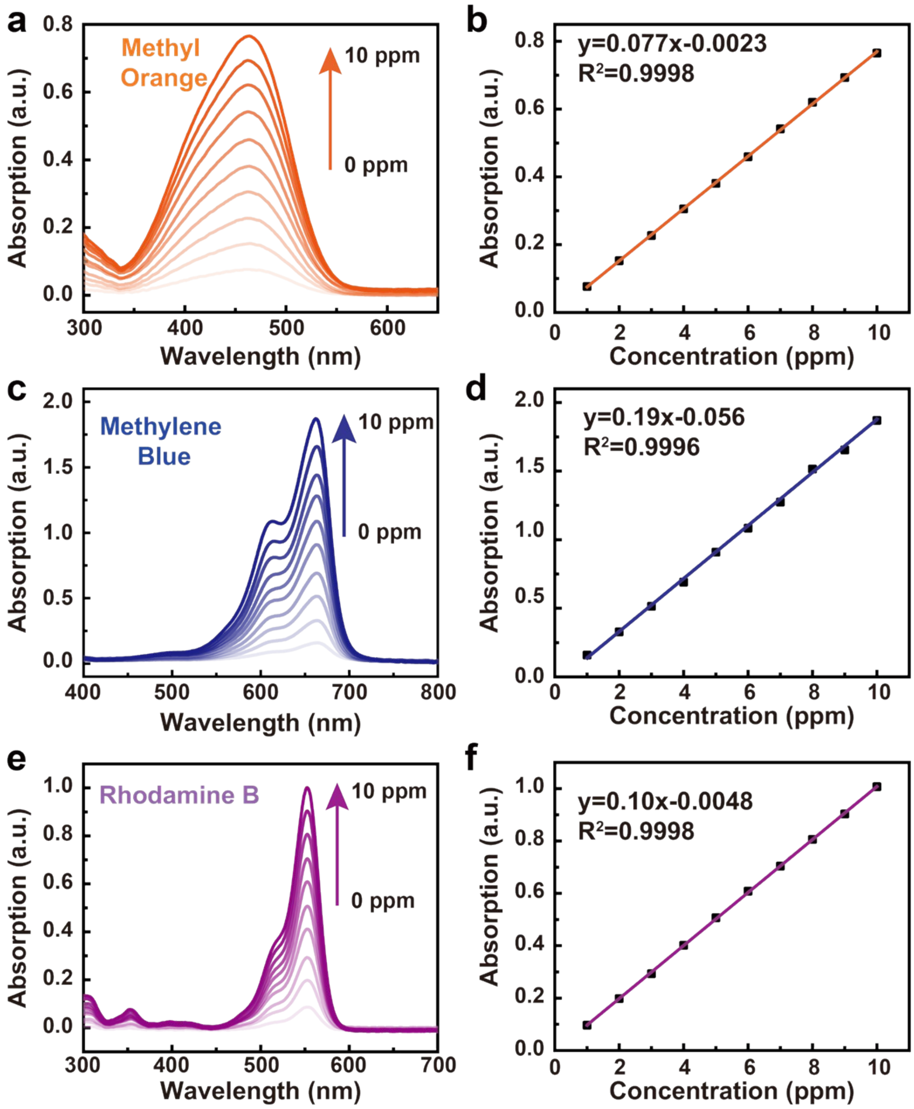

Fig. S19 Absorbance spectra of dye solutions at various concentrations, (a) MO, (c) MB, and (e) RhB. Linear correlation of the absorbance intensity to (b) MO concentration, (d) MB concentration, and (f) RhB concentration.

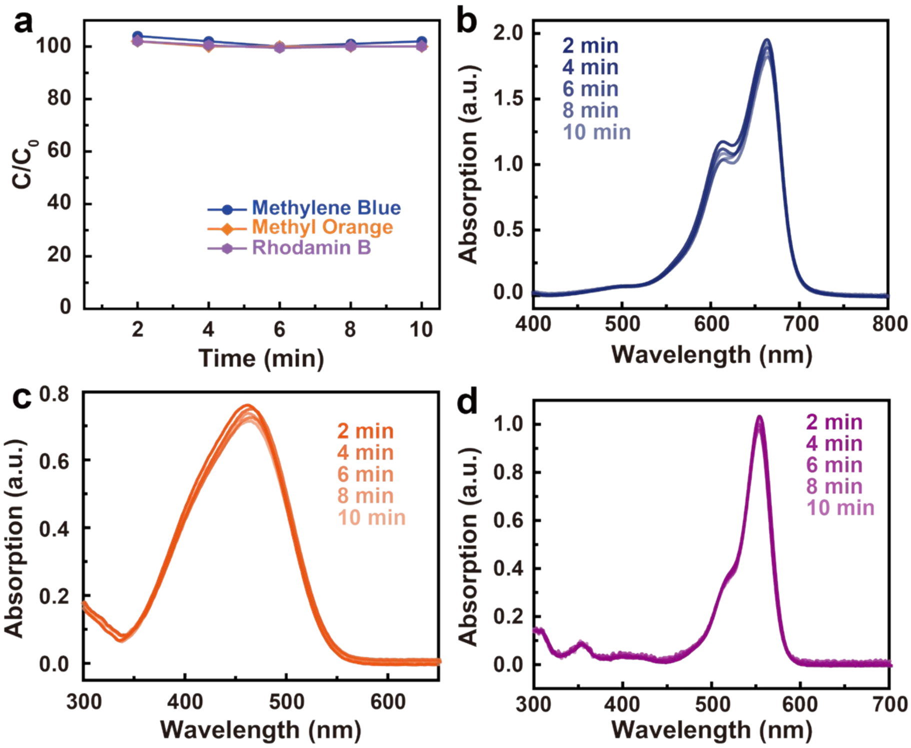

Fig. S20 (a) The dye concentration after adsorption saturation and the absorbance spectra of dye solutions, MO (b), MB (c), and RhB (d).

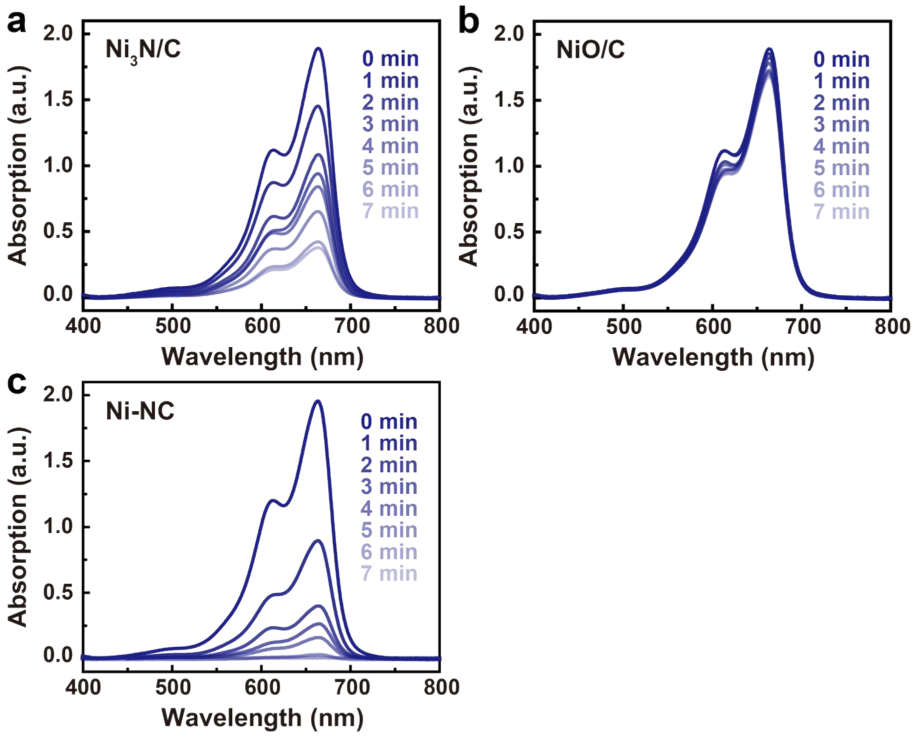

Fig. S21 The absorbance spectra correspond to the MB solution concentration under the Fenton-like performance of Ni_3N/C, NiO/C, and Ni-NC.

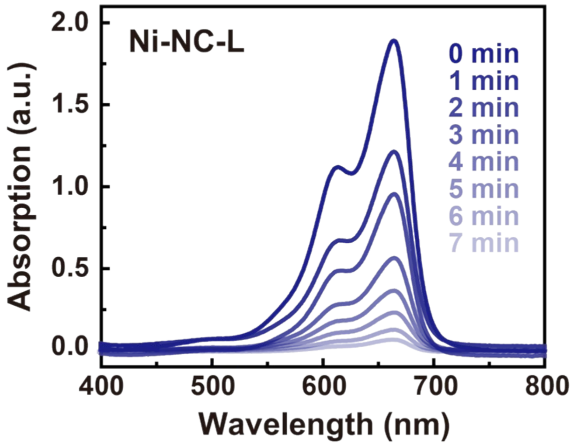

Fig. S22 The absorbance spectra correspond to the MB solution concentration under the Fenton-like performance of Ni-NC-L.

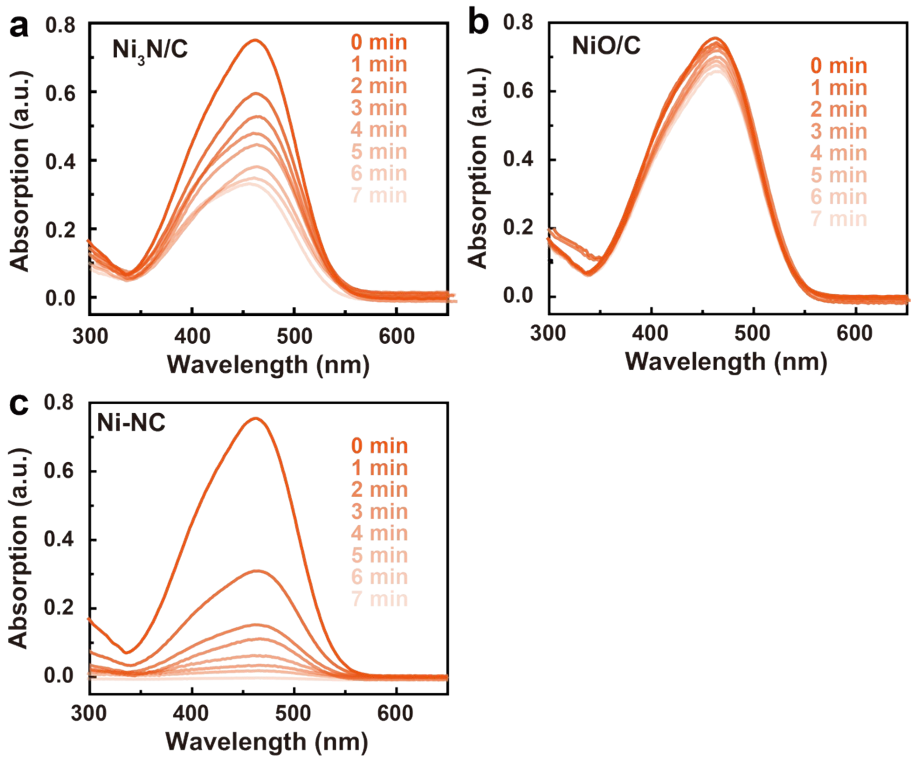

Fig. S23 The absorbance spectra correspond to the MO solution concentration under the Fenton-like performance of Ni_3N/C, NiO/C, and Ni-NC.

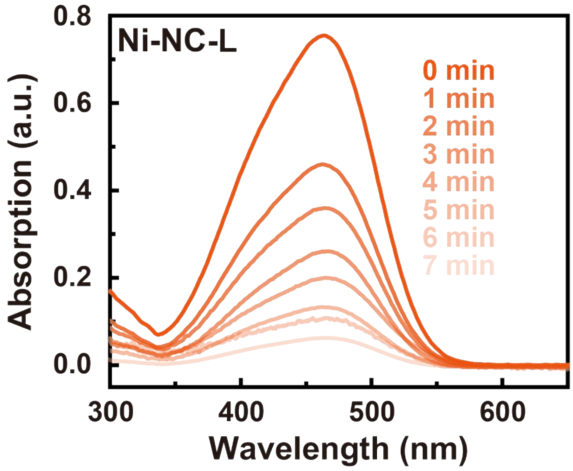

Fig. S24 The absorbance spectra correspond to the MO solution concentration under the Fenton-like performance of Ni-NC-L.

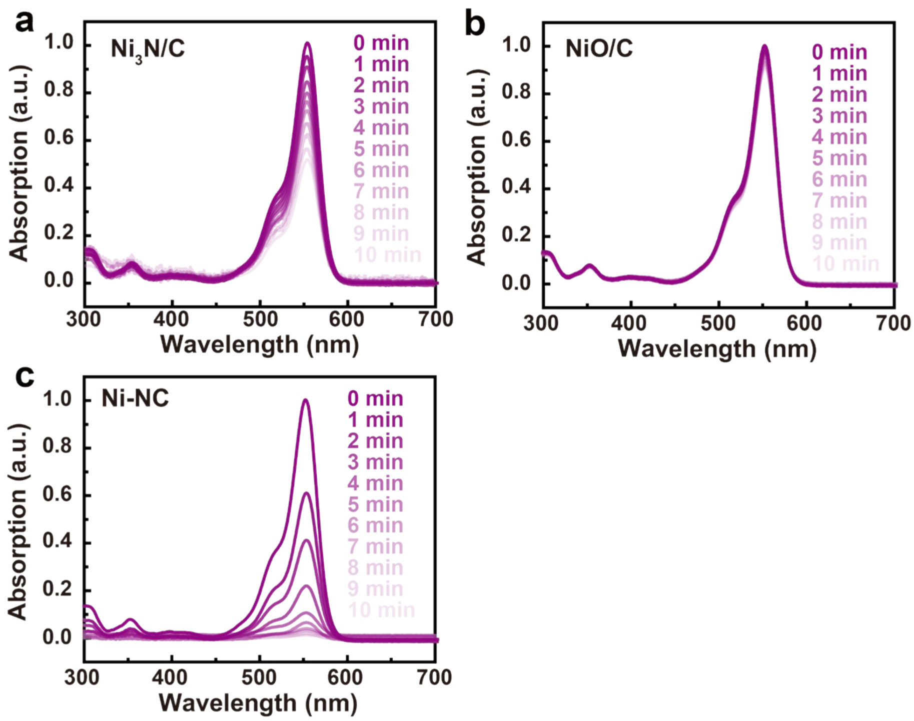

Fig. S25 The absorbance spectra correspond to the RhB solution concentration under the Fenton-like performance of Ni_3N/C, NiO/C, and Ni-NC.

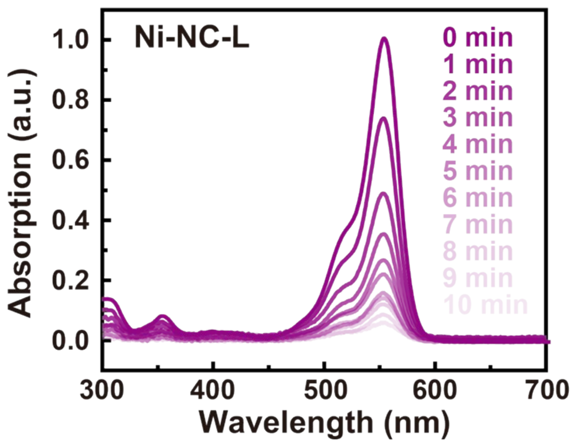

Fig. S26 The absorbance spectra correspond to the RhB solution concentration under the Fenton-like performance of Ni-NC-L.

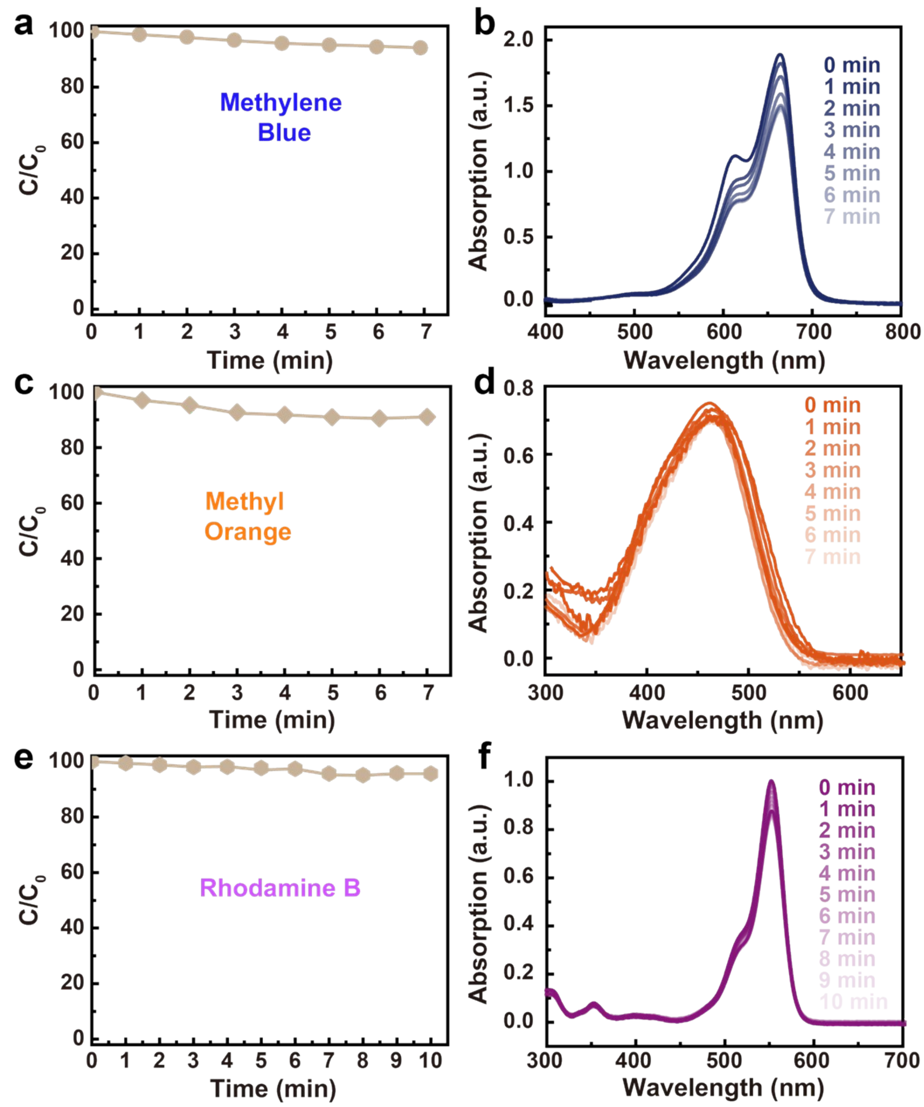

Fig. S27 Fenton-like performance of NC for various dye solutions, MB (a), MO (c), and RhB (e), and the corresponding absorbance spectra correspond to the dye solution concentration

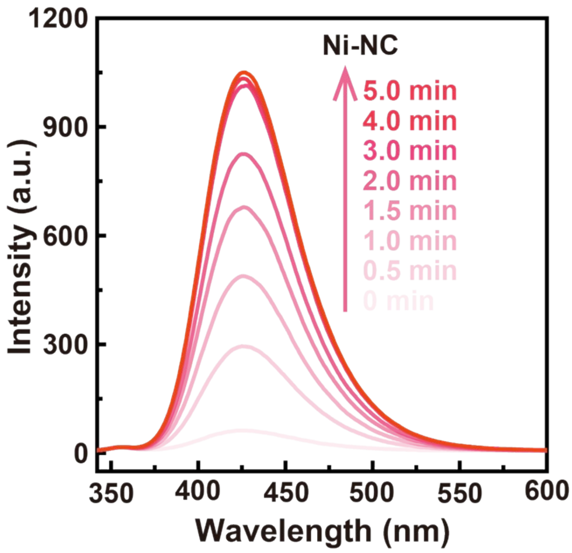

Fig. S28 The •OH generation of Ni-NC by using TA as a probe during different time.

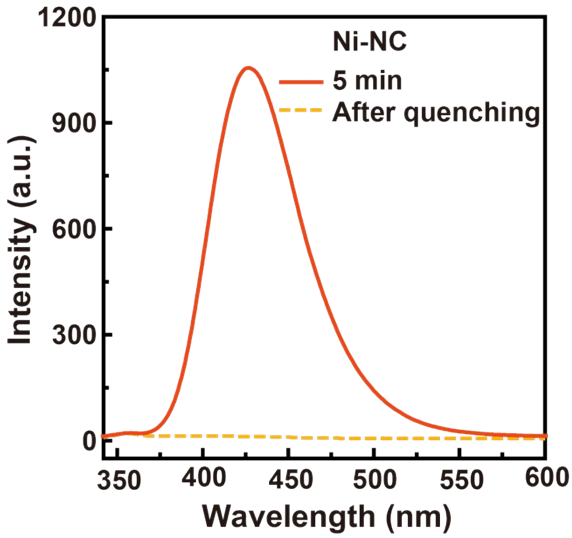

Fig. S29 Comparison of •OH generation of Ni-NC under MB degradation condition and after quenching.

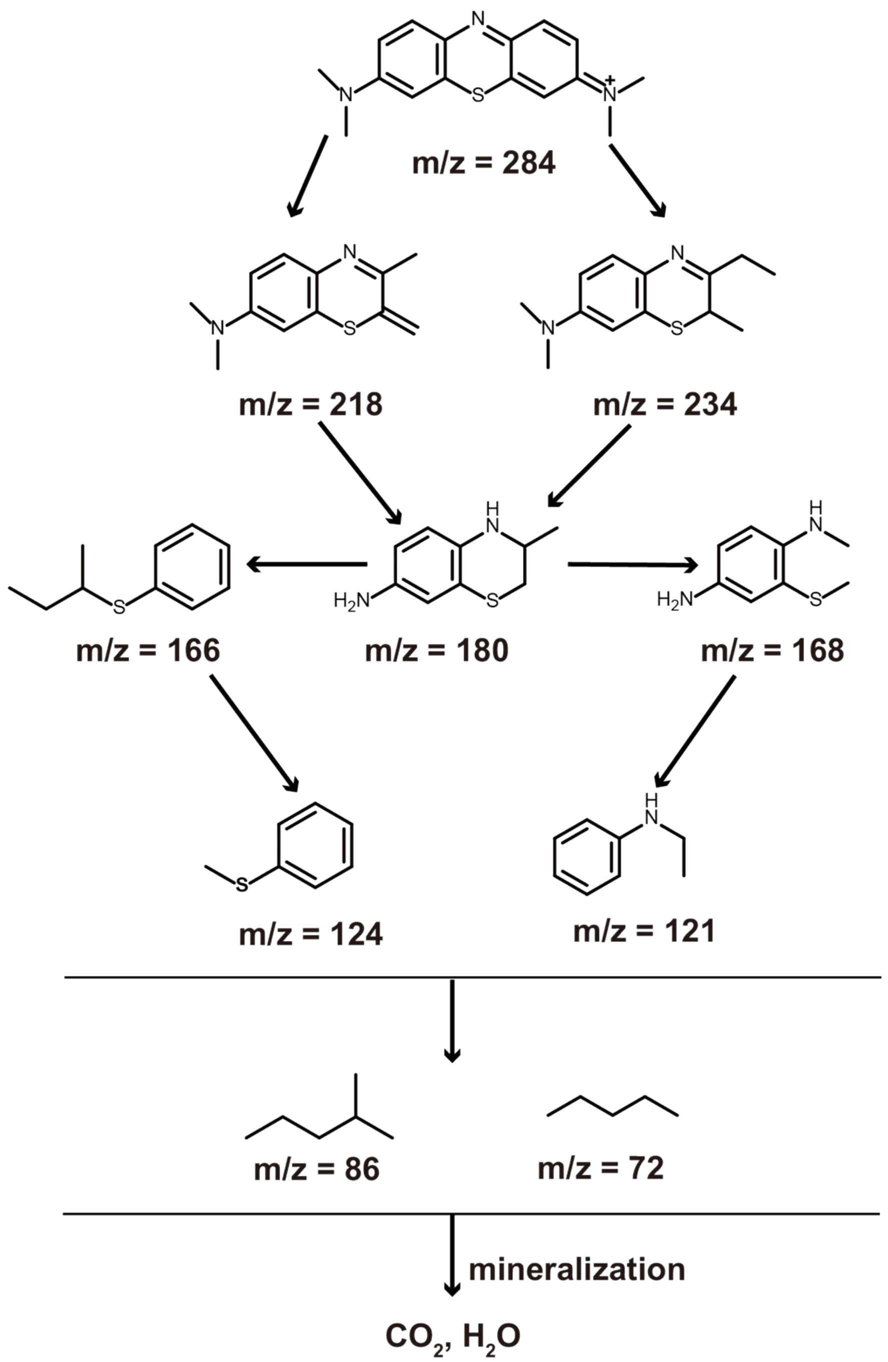

Fig. S30 Probable degradation pathway of MB.

Note: This degradation pathway is based on the analysis of the major peaks in the LC-MS chromatograms. Other non-detected reaction intermediates might also exist. The reaction intermediate for a certain m/z value shown here is just a selection among numerous possible molecules, especially for the intermediates of small m/z values.

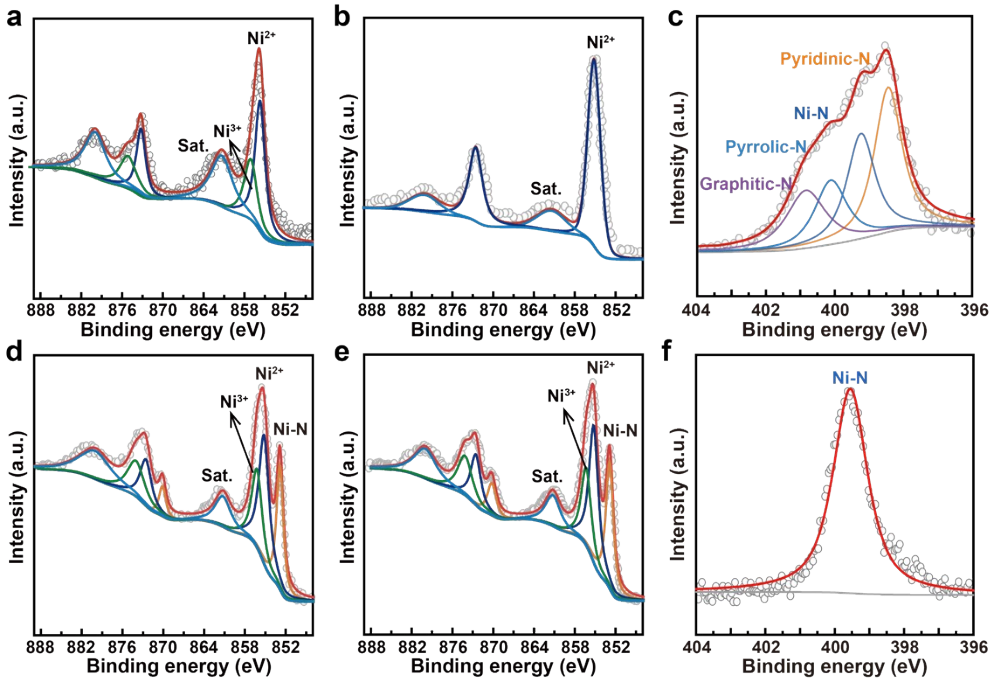

Fig. S31 XPS spectra of catalysts at various process. Ni 2*p* spectra of the catalysts when H_2O_2 was activated, (a) Ni-NC and (d) Ni_3N/C. Ni 2*p* spectra of the catalyst catalysts when adequent MB was degradation, (b) Ni-NC and (e) Ni_3N/C, and the corresponding N 1*s* spectra of (c) Ni-NC and (f) Ni_3N/C.

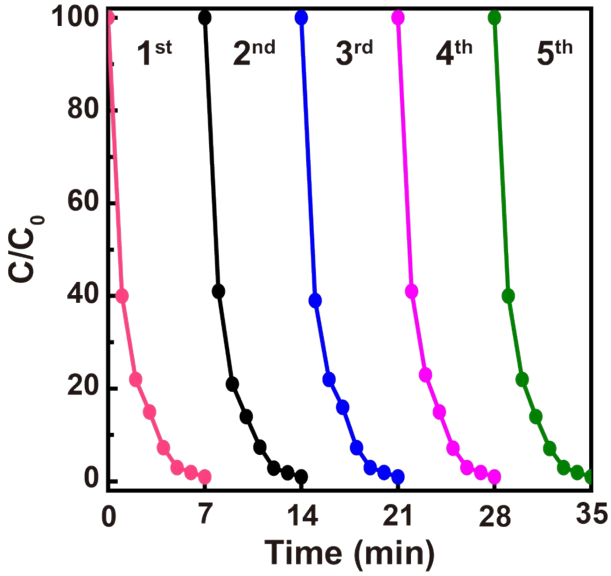

Fig. S32 The cyclic test of MB degradation reactions of Ni-NC.

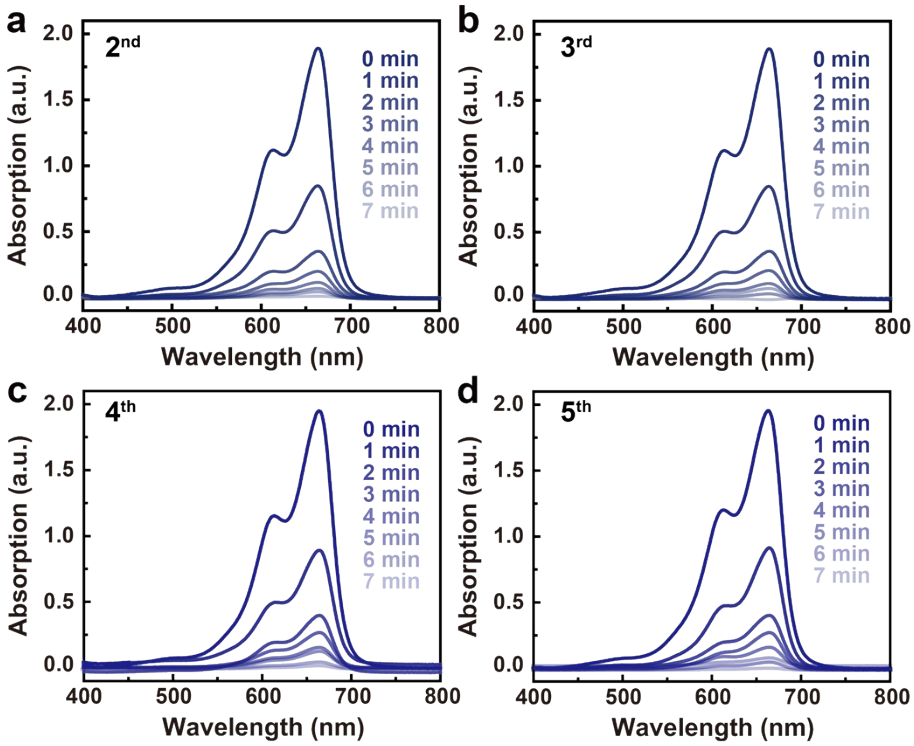

Fig. S33 The absorbance spectra correspond to the MB solution concentration under the Fenton-like performance of Ni-NC during 5 cycles.

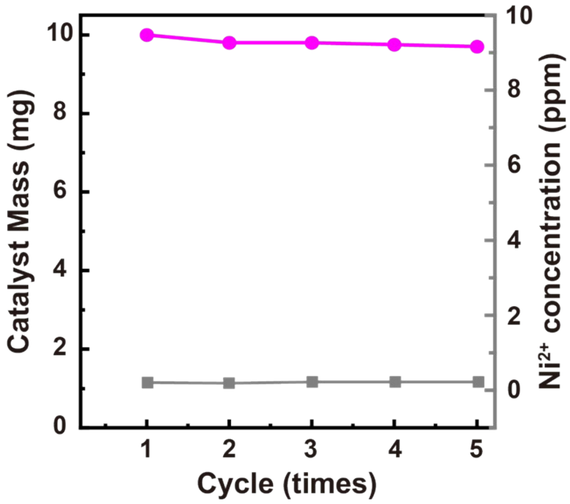

Fig. S34 The mass of Ni-NC and Ni^{2+} leaching concentration of Ni-NC during 5 cycles.

Table S1. The Ni content of all catalysts.

Catalysts	Ni content (wt.%)
Ni-NC-L	5.1
Ni-NC	9.3
Ni NPs/C	12.3
Ni_3N/C	10.2
NiO/C	15.6

Table S2. Parameters of EXAFS fittings for Ni-NC, Ni_3N/C, and reference samples (Ni foil and NiPc).

Sample	Shell	N^a	R (Å)^b	σ^2*10^{-3} (Å^2)^c	ΔE_0 (eV)^d	R factor
Ni-NC	Ni-N	4.0±0.7	1.41	7.5±0.6	5.9	0.0013
Ni_3N/C	Ni-N	1.7±0.7	1.42	6.4±0.5	4.6	0.0018
	Ni-Ni	10.3±0.7	2.29	9.5±0.8		
Ni foil	Ni-Ni	12	2.21	7.9±0.9	5.1	0.0019
NiPc	Ni-N	4.1±0.8	1.48	9.6±0.8	3.9	0.0012

^{a}*N*: coordination numbers; ^{b}*R*: bond distance; ^{c}σ^2: Debye-Waller factors; ^{d}ΔE_0: the inner potential correction; S_0^2=0.78.

Table S3. The comparison of catalytic performances for the recently reported Fenton-like catalysts.

Catalysts	Contaminant	$m_{catalyst}$ (mg)	C_{MB} (ppm)	C_{H2O2} (ppm)	k (min^{-1})	Ref.
Ni-NC	MB	10	20	10	0.767	This work
Ni-NC	MO	10	20	10	0.641	This work
Ni-NC	RhB	10	20	10	0.592	This work
Fe@N-C-800	MB	10	50	34	1.2	[1]
Fe@N-C-800	RhB	10	50	34	0.38	[1]
Cu/NC-MMT	RhB	20	20	800	0.595	[2]
Cu-C_3N_4	RhB	10	10	1000	1.64	[3]
MSO-12	MB	10	50	27	0.995	[4]
SA-Rh/NC	RhB	10	60	/	0.103	[5]
Fe-MG	MB	/	20	13.6	0.231	[6]
Co/Cu/zeolite	RhB	/	10	1020	0.053	[7]
Fe-BDC_1	RhB	/	20	1440	0.09	[8]
Fe SA/NPCs	RhB	/	25	/	19.657	[9]

References

1 L. Wang, L. Rao, M. Ran, Z. Wu, W. Song, Z. Zhang, H. Li, Y. Yao, W. Lv and M. Xing, *Nat. Commun.* 2023, **14**, 7841.

2 C. Gu, S. Wang, A. Zhang, C. Liu, J. Jiang and H. Yu, Proc. *Natl. Acad. Sci. U.S.A.* 2023, **120**, e2311585120.

3 J. Xu, X. Zheng, Z. Feng, Z. Lu, Z. Zhang, W. Huang, Y. Li, D. Vuckovic, Y. Li, S. Dai, G. Chen, K. Wang, H. Wang, J. K. Chen, W. Mitch and Y. Cui, *Nat. Sustain.* 2021, **4**, 233-241.

4 Y. Zheng, L. Wang, L. Zhang, H. Zhang and W. Zhu, Nano Res. 2022, **15**, 2977-2986.

5 S. Hu, J. Guan, R. Ma, Y. Tao, D. Liu, J. Gong and Y. Xiong, Rare Metals 2024, **43**, 2331-2338.

6 M. Zhou, W. Zhang, Z. Li, T. Feng, S. Lan, Z. Peng and S. Chen, *Rare Metals* 2023, **42**, 3443-3454.

7 X. Zhang, D. Ma and X. Zhu, *Environ. Eng. Res.* 2024, **29**, 230095-230104.

8 Q. Wu, M. Siddique, Y. Yang, M. Wu, L. Kang and H. Yang, *J. Clean. Prod.* 2022, **374**, 134033.

9 L. Yang, H. Yang, S. Yin, X. Wang, M. Xu, G. Lu, Z. Liu and H. Sun, *Small* 2022, **18**, 2104941.